DISCUSSION OF THE EVOLUTION OF MICRO CRACKS BY CHARACTERIZATION AND MODELING OF METAL MATRIX COMPOSITES REINFORCED BY METALLIC GLASS PARTICLES

K. Schulz, K. Lichtenberg and K.A. Weidenmann

Institute for Applied Materials, Karlsruhe Institute of Technology KIT,
Kaiserstr. 12, D-76131 Karlsruhe, Germany
Email: katrin.schulz@kit.edu, klaudia.lichtenberg@kit.edu, kay.weidenmann@kit.edu
Web page: http://www.iam.kit.edu

Keywords: micro crack initiation, micromechanical dislocation-based modeling, metal matrix composites, in-situ characterization

ABSTRACT

The development of innovative materials is a base technology for the development of novel components preserving energy and resources. Composites allow for tailoring the desired materials properties beyond the performance of bulk materials. Nevertheless, the reliable design and construction of components made from composite materials needs profound knowledge about the damage mechanisms. To develop reliable material and damage models, a detailed characterization and a physically defined description of the mechanics of the composite materials is of major importance. For metal matrix composites the reinforcement of a relatively soft matrix material with hard particles is state-of-the-art. A novel approach for such composites presented by the authors is the use of metallic glass particles. Up to now, such composites have been predominantly produced by powder metallurgy, but increasing the crystallization temperature of metallic glasses, i.e. in the system NiNbX (X=Sn,Ta), allows for liquid metal infiltration to produce metallic glass reinforced metal matrix composites (MMCs).
In this contribution, investigations on the micro crack evolution in MMCs reinforced with metallic glasses made from the above-mentioned alloys are presented. As the glass is manufactured as thin ribbons in a melt-spinning process, the particle architecture is a plate-like one resulting in notch effects on the plate edges as the particles are made by grinding the ribbons. In fact, the potential influence of this effect on the damage behavior of these composites is investigated in this contribution by means of in-situ characterization of the composites under compression. This method allows for detecting the sites of micro crack initiation in the composite's microstructure and observing the crack propagation under quasi-static loading conditions. The results from the materials characterization are compared to numerical experiments. A dislocation-based continuum model is adopted to the microstructure and allows to investigate the interaction between the hard amorphous particles and the surrounding aluminum matrix. Local stress concentrations are analyzed which occur in these composites due to inhomogeneous dislocation movement and hence cause plastic deformation and crack initiation in the composite material.

1 INTRODUCTION

1.1 MMCs based on metallic glasses

Metallic glasses have already been known for their outstanding properties since several years. Elastic strain limits up to 2 % [1] and high strength values (~ 3 GPa for Ni-based [2], ~ 4 GPa for Fe-based [3] and ~ 5 GPa for Co-based [4] metallic glasses) were reported in various studies. But industrial application of metallic glasses is mostly limited due to their brittleness [5]. By incorporating the metallic glasses as reinforcements in metal matrix composites (MMCs), brittleness can be averted by surrounding plastic flow within the matrix materials as it has already been reported for ceramic reinforcements [6, 7].

Newly developed Ni-based metallic glasses exhibit high thermal stability and crystallization temperatures up to 994 K [8]. Therefore, they offer high potential for being embedded as reinforcements

in lightweight metal alloys not only by sintering methods but now also by melt infiltration since crystallization temperatures are higher than melting temperatures of several lightweight alloys. In the infiltration process, a preform or mold filled with particles or fibers is infiltrated with a molten metal. Recent studies show that production of MMCs with structures of metallic glass by melt infiltration is possible without crystallization of the glass [9, 10]. Furthermore, these studies present that the composites offer higher strength values than the bulk matrix material regardless of processing method [9, 10, 11].

The reinforcing effect of metallic glass is likely to be supported by the good interfacial bonding between the metallic glass and the metallic matrix material. Cytron et al. showed that 180° bending tests lead to cracks within the metallic glass but not in the interface. SEM investigations of metallic glass particle reinforced MMC samples after a compression test presented by Scudino et al. [13] display several damage mechanisms. In their study, fracture appears parallel to the compression direction in the reinforcing particles while large plastic deformation with dimple rupture takes place in the Al-matrix.

Within the present study, in-situ compression tests within a SEM chamber will be performed for a detailed investigation of the damage evolution in metallic glass particle reinforced MMCs produced by gas pressure infiltration. The results of the damage analysis are then compared to predictions based on a dislocation-based continuum model.

1.2 Dislocation-based continuum models

The growing interest in physically motivated continuum models of plasticity has led to renewed efforts to formulate continuum theories of dislocation kinematics and dynamics. The classical continuum theory of dislocation based plasticity, which is based on the definition of a second-rank dislocation density tensor, was introduced by Kröner [14] in the 1950s. However, the classical density tensor only captures some aspects of plastic deformation processes. Introduced as a measure of the averaged plastic deformation state to link the microscopically discontinuous deformation state to a macroscopically continuous deformation state, the classical density tensor just considers the dislocation content in an averaging volume and thereby only accounts for geometrically necessary dislocations (GNDs) and does not account for statistically stored dislocations (SSDs).

In order to solve this problem, the classical model has been extended by Hochrainer et al. [15] by means of a geometrical description of dislocation lines and their averages under consideration of a higher dimensional configuration space. They give the mathematical foundations for using the methods of statistical mechanics consistently with three-dimensional systems of curved dislocations. This higher dimensional continuum dislocation dynamics theory (hd-CDD) relies on a geometrical description of dislocation lines and their averages, i.e. line densities, which uses the methods and formalisms of differential geometry. The theory is a direct generalization of Kröner's classical continuum theory, which is contained as a special case. Having formulated the kinematic problem, one can combine hd-CDD with a constitutive relation for the dislocation velocity, as demonstrated for simple systems in Schulz et al. [16].

In recent years, composite materials have gained increasing attention. To understand the complex material behavior of solids with more than one phase, Van der Giessen et al. [17] analyzed a two phase composite using a discrete dislocation dynamics model. They simplified the system as a 2D plane strain problem considering edge dislocations on parallel slip planes only. Slightly different systems based on discrete dislocation analyses have been presented by Cleveringa [18, 19] and Schwarz et al. [20]. A comparison of a nonlocal statistical-mechanics model with the discrete results of Cleveringa [18, 19] is given by Yefimov et al. [21].

In this paper, we discuss the numerical continuum formulation based on the mathematical model given in Hochrainer et al. [22] by applying it to a composite material. We thereby show that we can reproduce the plastic material behavior considering different boundary conditions and we are able to represent the dislocation pile-up at the interfaces. Beyond we show the influence of the shape and position of the inclusions on the evolution of the plastic slip.

2 EXPERIMENTAL

2.1 Specimen material

The metallic glass particle reinforced MMC experimentally investigated in this study was fabricated by gas pressure infiltration. Aluminum alloy AlSi12 was used as matrix material and metallic glass $Ni_{60}Nb_{20}Ta_{20}$ particles as reinforcements. The metallic glass particles were prepared by milling of thin melt-spun ribbons. Therefore, the used particles exhibit a platelet-like shape with a size range of 0.6 to ~ 2 mm and a thickness of ~ 50 μm.

For processing, an alumina crucible with a graphite mold filled with glass platelet was placed into the infiltration chamber together with ingots of AlSi12. After evacuation and several intermediate Argon flushing steps, the infiltration chamber was heated to the processing temperature T_p = 660 °C. This temperature was held for two hours. Thereafter, infiltration pressure of 40 bar Argon was applied and held while cooling down the infiltrated sample. As presented in [10], this results in a metallic glass particle reinforced MMC without crystallization of the metallic glass. The average volume content of metallic glass platelets in the MMC was determined to 12.1 vol.% via Archimedes' principle method. For a more detailed description of the gas pressure infiltration process, device and processing parameters and the composite material, the authors refer to [23] and [10].

2.2 Mechanical testing and microstructural investigations

The damage mechanisms of the presented metallic glass particle reinforced MMC were investigated under compressive load. The mechanical tests were carried out inside a scanning electron microscope (SEM) chamber for direct observation of microstructural changes while testing. This allows for accurate determination of the failure mechanisms though obtained information is limited to the specimen surfaces.

Compression tests were performed using a miniature mechanical testing device by Kammrath & Weiss GmbH (Dortmund, Germany) with maximum load capacity of 10 kN. Elongation was measured by the displacement of the crossheads. All experiments were performed with a fixed crosshead velocity of 2 μm/s which corresponds to a nominal strain rate of approximately 10^{-3}/s. In-situ investigation of the damage mechanisms was carried out in a Zeiss EVO 50 scanning electron microscope (SEM). Stopping the mechanical tests at different loads allowed for detailed examination of the damage mechanisms and the damage evolution of the MMC.

Rectangular parallelepiped testing samples with a side length of ~2 mm were used for the compression tests. The samples were prepared out of the infiltrated specimen by electrical discharge machining. All samples were grinded with SiC paper with 4000 abrasive grit and water as coolant. Afterwards, the samples were polished with 3 μm diamond suspension for sufficient surface quality.

Within the composite, the platelets mostly seem to be oriented perpendicular to the infiltration direction due to the plate-like shape of the particles as shown in [10]. Compression tests in the present contribution were carried out along the platelet orientation (cf. Figure 1).

3 MODELLING

3.1 Dislocation-based continuum model

The idea of the continuum dislocation dynamics (hd-CDD) model is that dislocation lines can be distinguished according to their line direction l. This assumption enables us to include not only geometrically necessary dislocations but also statistically stored dislocations, which, considering an averaging volume, do not have the same orientation. Provided that dislocations move by glide only, we introduce the orientation angle φ between the line direction and the Burgers vector b. With this angle, a point r of a dislocation is characterized by (r,φ). For every dislocation curve c=(c1(s), c2(s)) (straight or curved), which is parametrized by the arc length s, we now get an artificially lifted curve C(s)=(C1(s), C2(s), C3(s)):=(c1(s), c2(s), φ(s)) in the three dimensional configuration space. Here the 1-direction points into the direction of b and the glide plane is spanned by the 1- and 2-direction. An important feature of the hd-CDD model is that in the following we average over these lifted curves. The tangent of the lifted curve is given as

$$\frac{d\boldsymbol{C}}{ds} = \left(\frac{d\mathbf{c}^1}{ds}, \frac{d\mathbf{c}^2}{ds}, \frac{d\varphi}{ds}\right) = \left(\frac{d\mathbf{c}}{ds}, k(s)\right)$$

Here, we derive as third coordinate the curvature k(s) of the curve $\mathbf{c}$. Similar to the classical dislocation density tensor $\boldsymbol{\alpha}$, given by Kröner [14], we introduce a dislocation density tensor of second order $\boldsymbol{\alpha}^{II}_{(r,\varphi)}$, with

$$\boldsymbol{\alpha}^{II}_{(r,\varphi)} = \langle \textstyle\sum_{C} \delta_C \frac{d\boldsymbol{C}}{ds} \otimes \boldsymbol{b} \rangle,$$

considering the lifted dislocation curves in an averaging volume. This expression can be replaced by the product of the generalized line direction $\boldsymbol{L}_{(\mathbf{r},\varphi)} = \boldsymbol{l}_{(\varphi)}, k_{(\mathbf{r},\varphi)}$ in the higher order configuration space and a dislocation density function $\rho_{(\mathbf{r},\varphi)}$ as

$$\boldsymbol{\alpha}^{II}_{(r,\varphi)} = \rho_{(\mathbf{r},\varphi)} \boldsymbol{L}_{(\mathbf{r},\varphi)} \otimes \boldsymbol{b} = \rho_{(\mathbf{r},\varphi)} \begin{bmatrix} b^1 cos\,\varphi & b^2 cos\,\varphi \\ b^1 sin\,\varphi & b^2 sin\,\varphi \\ b^1 k_{(r,\varphi)} & b^2 k_{(r,\varphi)} \end{bmatrix}$$

According to the classical continuum approach, the fundamental condition div $\boldsymbol{\alpha}^{II}_{(r,\varphi)} = 0$ has to be fulfilled in hd-CDD which ensures that no dislocation lines start or end inside a crystal. This condition can be rewritten as $cos\,\varphi\,\partial_x\rho + sin\,\varphi\,\partial_y\rho + \partial_\varphi(\rho\,k) = 0$.

The evolution of the density tensor $\boldsymbol{\alpha}^{II}_{(r,\varphi)}$ can be obtained as $\partial_t\boldsymbol{\alpha}^{II}_{(r,\varphi)} = -\text{curl}(\boldsymbol{V}_{(r,\varphi)} \times \boldsymbol{\alpha}^{II}_{(r,\varphi)})$. Here, the vector $\boldsymbol{V}_{(r,\varphi)} = (\boldsymbol{v}_{(r,\varphi)}, \boldsymbol{\vartheta}_{(r,\varphi)})$ denotes the generalized velocity in the configuration space, which is perpendicular to the generalized line direction. $\boldsymbol{v}_{(r,\varphi)}$ describes the spatial velocity and $\boldsymbol{\vartheta}_{(r,\varphi)}$ the rotational velocity, respectively. Assuming that dislocations move on glide planes only, we can replace the evolution of $\boldsymbol{\alpha}^{II}_{(r,\varphi)}$ by two scalar evolution equations for the dislocation density $\rho(r, \varphi)$ and the mean curvature $k(r, \varphi)$ of the dislocation lines.

$$\partial_t\rho = -\left(div\,(\rho\,\mathbf{v}) + \partial_\varphi(\rho\,\boldsymbol{\vartheta})\right) + \rho\,\mathbf{v}\,k$$
$$\partial_t k = -vk^2 + \nabla^2_L(\boldsymbol{\vartheta}) - \nabla_{V(k)}$$

Whereas $\mathbf{v}$ denotes the spatial velocity, v here represents the scalar velocity of a dislocation segment. ∇_V and ∇^2_L describe the first derivative along the generalized velocity and the second derivative along the generalized line direction, respectively.

The evolution of the plastic distortion $\boldsymbol{\beta}^{pl}$ can be derived by an integral over the angle φ as

$$\partial_t\boldsymbol{\beta}^{pl} = \int_0^{2\pi} \rho_{(r,\varphi)}\,v_{(r,\varphi)}d\varphi\,\boldsymbol{n}\otimes\mathbf{b}$$

which is similar to the Orowan relation. For a more detailed description see Hochrainer et al. [22].

In order to provide an effective analysis for a broad range of applications, the computation time and storage capacities of the higher dimensional continuum theory can't be neglected. A number of benchmark tests showed that the hd-CDD theory is computationally intensive caused by the high amount of degrees of freedom. Thus there might be the need of a reduction of degrees of freedom at preferably same performance in order to have the chance to consider larger and more complex systems. In the following analysis we use a simplified version of CDD. By partially integrating the governing evolution equation of the higher order theory, we decrease the number of unknowns per glide system. At this, we obtain the internal variables from integration over the orientation space, characterized by the angle φ. Thus, for a single glide system, the total dislocation density ρ^t is derived by

$$\rho_{(r)}^t = \int\limits_0^{2\pi} \rho_{(r,\varphi)} \mathrm{d}\,\varphi\,.$$

As part of the total dislocation density, the density of the geometrically necessary dislocations ρ^{GND} is introduced. It holds

$$\rho^{GND} = \sqrt{(\bar{\rho}^1)^2 + (\bar{\rho}^2)^2} \quad \text{with} \quad \begin{aligned} \bar{\rho}^1 &= \int\limits_0^{2\pi} \rho_{(r,\varphi)} \cos(\varphi)\,\mathrm{d}\,\varphi \\ \bar{\rho}^2 &= \int\limits_0^{2\pi} \rho_{(r,\varphi)} \sin(\varphi)\,\mathrm{d}\,\varphi. \end{aligned}$$

For brevity, in the following we only state the resulting evolution equations for a glide plane which depends on x only. The evolution equations for ρ^t and ρ^{GND} are given as

$$\partial_t \rho^{GND} = -\partial_x\, \rho^t v$$
$$\partial_t \rho^t = -\partial_x(v\,\rho^{GND}) + v\,\rho^t k$$

with the scalar dislocation velocity v and the mean curvature k of the dislocation lines. The term including the curvature accounts for the change of the density due to expansion or shrinking of dislocation loops. The evolution equation for k we can write as

$$\partial_t k = -v\,k^2 - \frac{\rho^t - \rho^{GND}}{2\,\rho^t}\,\partial_{xx}\,v + \frac{\rho^{GND}}{\rho^t}(k\,\partial_x\,v - v\,\partial_x\,k)$$

The plastic slip γ on the slip plane causes a plastic distortion of the crystal. This plastic distortion can be written with the sum over all slip planes as $\boldsymbol{\beta}^{pl} = \sum_s \gamma_s/b_s \cdot (\boldsymbol{n} \otimes \boldsymbol{b})$. The evolution of the plastic slip we derive as $\partial_t \gamma = \rho^t b\,v$. Although we only use the case of k=0 for the numerical examples in this paper, cp. Groma et al. [24], a general 3D consideration with $k \neq 0$ is straight forward.

3.2 Finite element approximation

We implemented the dislocation based continuum model into a finite element code using quadrilateral four node elements with bilinear shape functions. According to the simplified kinematic assumption of small strains, the presented numerical analysis is geometrically linear. We imply an additively decomposition of the strain tensor by $\varepsilon = \varepsilon^{el} + \varepsilon^{pl}$.

Regarding the constitutive equations, it holds $\sigma = \mathbb{C} : \varepsilon^{el} = \mathbb{C} : (\varepsilon - \varepsilon^{pl})$. The fourth order tensor $\mathbb{C}$ here denotes the three dimensional elasticity matrix. CDD is combined with the dislocation velocity v. We use a linear-viscous model of overdamped dislocation motion, in which the dislocation velocity v depends on the difference between the local shear stress τ and the local yield stress τ_y. With the drag coefficient B for the dislocations, the velocity law holds

$$v = \begin{cases} b\,B^{-1}\,\mathrm{sign}(\tau)(|\tau| - \tau_y) & \text{if } |\tau| > \tau_y \\ 0 & \text{otherwise} \end{cases}$$

Herein, the yield stress $\tau_y = aGb\,\sqrt{\rho^t}$ depends on a geometry-dependent parameter $a \approx 0.4$ characterizing the strength of dislocation forest interactions, the shear modulus G, the Burgers vector b, and the total dislocation density. With the external stress τ_{ext} and the internal stress τ_{int}, including e.g. the backstress $\tau_b = DGb\,(\partial_x\,\rho^{GND}/\rho^t)$, cf. Zaiser et al. [25], considering the repelling effect of dislocations with same orientation, the shear stress can be derived by $\tau = \tau_{ext} - \tau_{int}$. Regarding the slip planes, which dislocations move on, we introduce representative slip planes, considering a bundle of parallel nearby slip planes. Therefore we choose a multi-scale approach with a finite difference (FD) scheme for approximating derivatives on the slip planes and a finite element (FE) mesh for the struc-

tural analysis. Hereby, the external stresses are projected from the FE mesh to the FD scheme as well as the stresses, arising from the motion of dislocations in the other direction. For the numerical time integration of the evolution equations we use an explicit forward Euler scheme in order to avoid additional history variables and to procure a fast computation.

4 RESULTS

4.1 In-situ compression tests

Figure 1 shows the compressive stress-elongation plot of an infiltrated metallic glass reinforced MMC sample tested along the platelet orientation (cf. Figure 1 (right, a)). The initial curved shape of the plot at small stresses can be attributed to friction between the sample and the punches and to the deviation of the sample geometry from perfect parallelism. The slope of the MMC increases steeply and changes over to almost ideal plastic deformation behavior. The tips within the plot mark stopping points of the compression test for SEM investigation of the damage evolution. The letters in the plot correspond to the letters on the micrographs which are presented in this contribution (cf. Figures 2 and 3). The test was terminated at the elongation of 200 μm when macroscopic cracks and massive plastic deformation were observed as shown in Figure 1 (right, d).
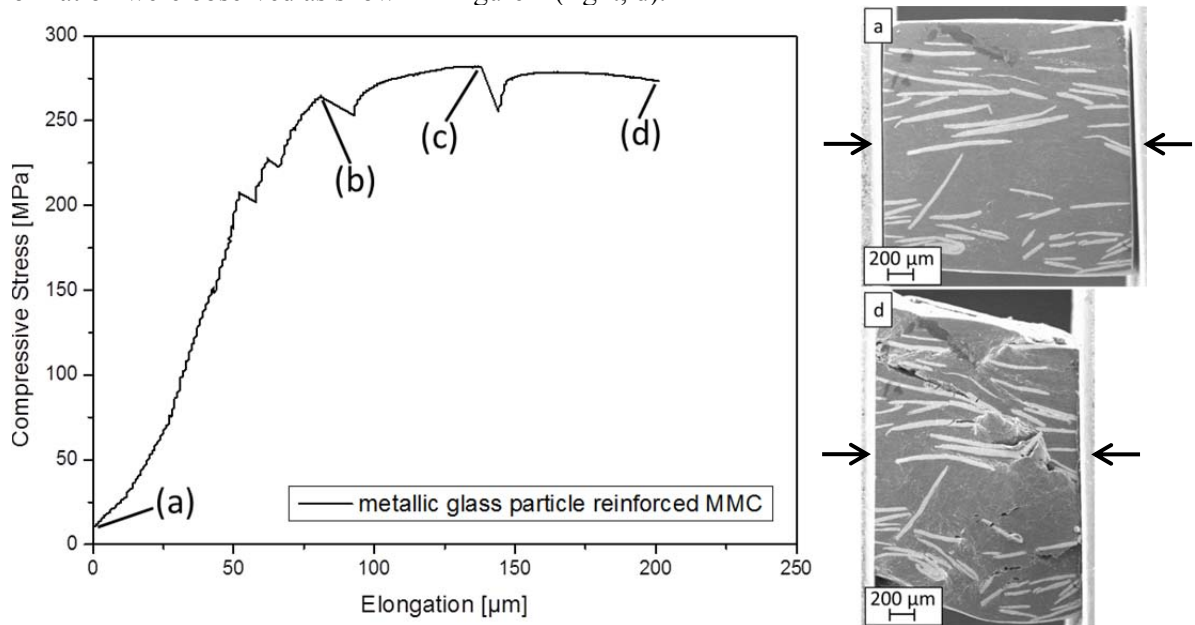

Figure 1: Compressive stress-elongation plot of an infiltrated metallic glass reinforced MMC sample, tested under uniaxial compression along the platelet orientation (left) and micrographs of a sample before (right, a) and after the compression test (right, d).

The SEM micrographs of the damage evolution at different loading steps are presented in the following. Metallic glass platelets appear as bright lamellae-like structures in the surrounding darker matrix metal. As the actual composition of the matrix alloy is hypereutectic, the matrix consists of an irregular eutectic microstructure with silicon primary crystals.

Figure 2 shows two SEM images which present an overview of the microstructure of the metallic glass particle reinforced MMC at different stages of the compression test. At stopping point (b), the microstructure of the MMC seems to be almost completely undamaged with no macroscopic deformation. Several microscopic cracks, which are marked with arrows in the micrograph (Figure 2 (b)), can be observed in this picture. With further elongation, the existing cracks within the matrix material get larger and wider, macroscopic crack propagation appears within the matrix and new cracks are generated in the metallic glass platelets. The new cracks are marked with arrows in Figure 2 (c). Furthermore, a concentration of plastic matrix deformation can be observed at the edge of a metallic glass platelet as shown in detail in Figure 3 (c) resulting in the formation of extrusions. The image shows that the metallic glass platelet cracked close to the extrusion and that there is crack propagation in the

interface between platelet and matrix material.

At the end of the compression test at point (d), macroscopic crack formation around the extrusion is observed as shown in Figure 3 (d). The existing cracks in the platelet and the interface got larger and wider with further elongation.
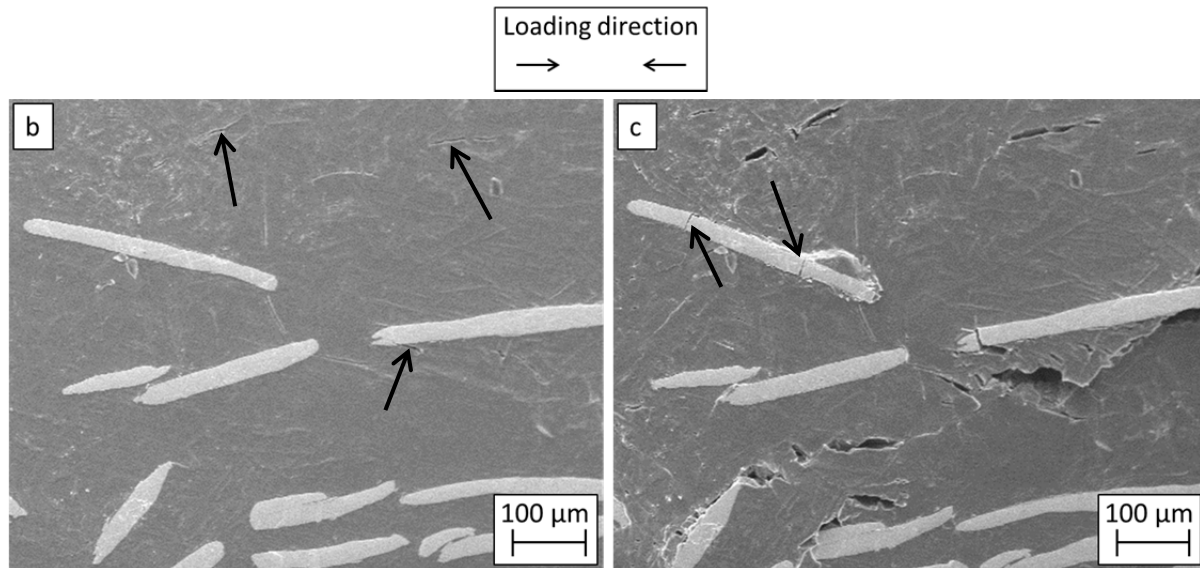

Figure 2: Damage evolution in the metallic glass particle reinforced MMC at different steps of the compression test – overview.
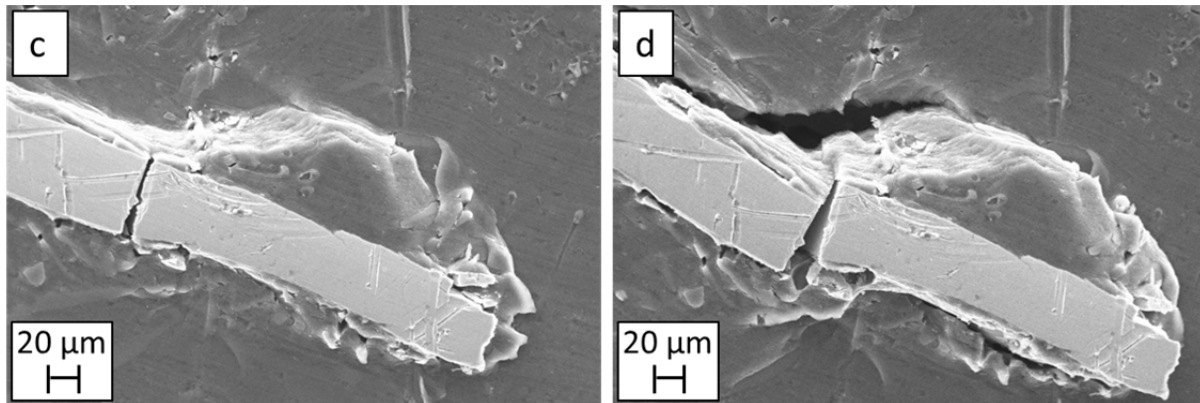

Figure 3: Development of extrusions due to dislocation pile-up at high loads and elongations – detailed micrographs at different stopping points of the compression test.

4.2 Modelling

We model a simplified composite material, consisting of a plastically deforming matrix and stiff inclusions (corresponding to the metallic glass platelets), which are impenetrable for dislocations. Hereby we concentrate on different boundary conditions, occurring dislocation pile-up effects, and the influence of the shape of the inclusion.

According to the dislocations, we model the boundary conditions with smooth boundary functions for the dislocation density ρ and the dislocation velocity v. These functions decay for the case that the boundaries are impenetrable for dislocations. For simplicity we focus on simplified material partitions of the composite, see Figure 4.
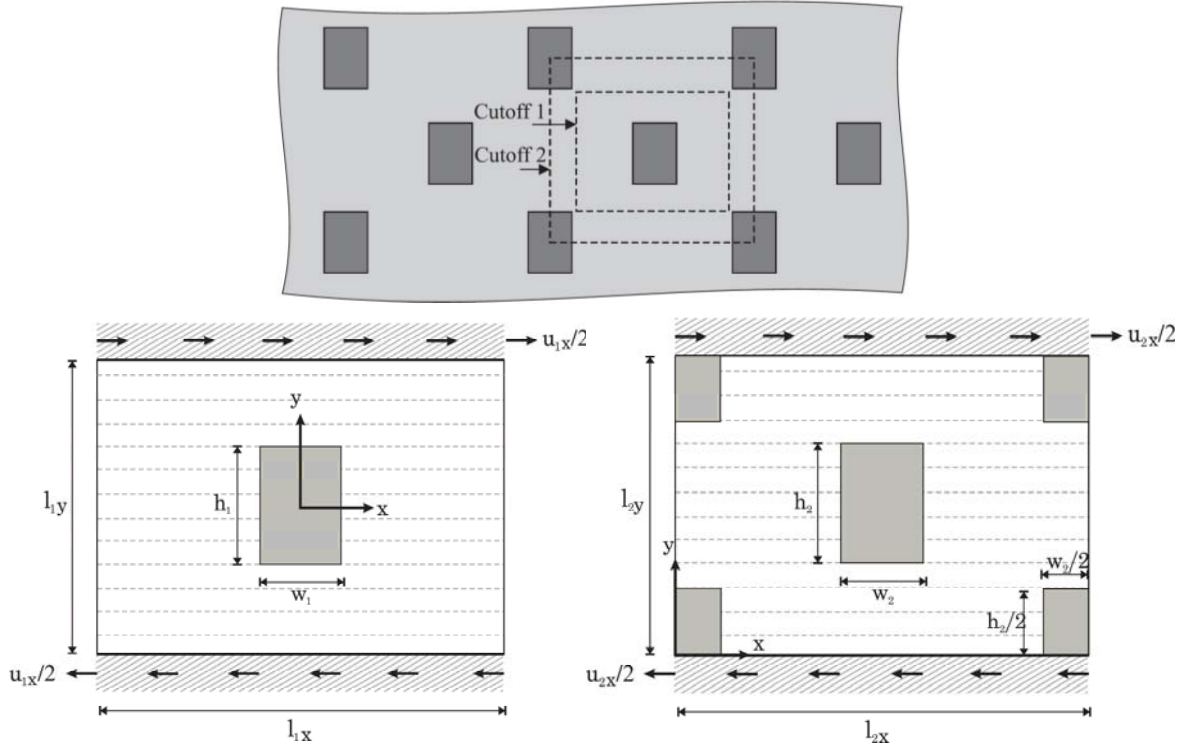
Figure 4: Simplified composite structure with different cutoff systems and variation of the inclusion geometry.

We differentiate between three geometries and analyze a matrix incorporating a single particle (System I), a matrix with five not overlapping particles (System II), and a matrix with five overlapping particles (System III). The quadratic systems has an edge length $l_{1x} = l_{1y} = 0.625 \cdot l_{2x} = 0.625 \cdot l_{2y} = 2$ µm. The material parameters for the isotropic aluminum matrix are given with the elastic modulus E=67.6 GPa and the Poisson's ration ν=0.3. For the inclusion it holds $E^{inc} = 7.3 \cdot E$ and $\nu^{inc} = \nu/2$. Parallel to the x axis, we assume a homogeneous distribution of 100 glide planes over ly and a Burger's vector b_x=0.2864 nm. By applying a prescribed displacement $u_x/2$ at the upper and the lower boundary, we subject the composite to a total shear deformation of u_x=2 nm. Regarding the dislocation microstructure, we assume an initial configuration of statistically stored straight edge dislocations (SSDs) only. The total dislocation density is assumed as $\rho_{tot} = 1013$ m^{-2}, the geometrically necessary dislocation density and the curvature vanish, ρ_{GND}=k=0. The system is modelled by using 32 x 32 elements for the FE mesh and 1000 elements for the FD scheme along the slip planes.
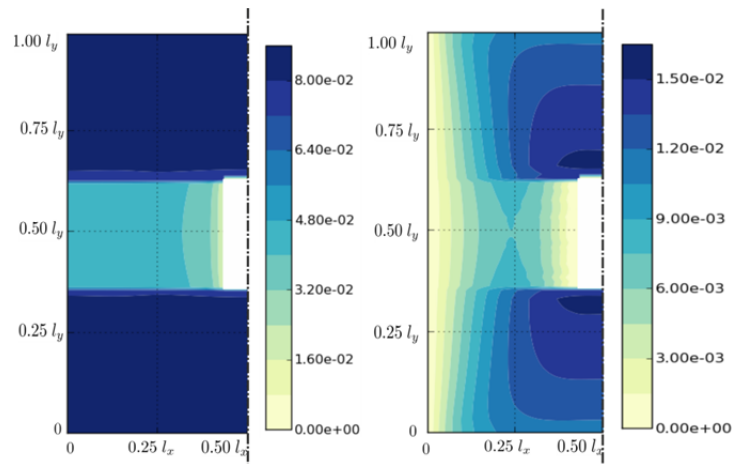

Figure 5: Contour plots of plastic slip for different boundary conditions on the left and right edge: periodic (left) mechanically free, impenetrable for dislocations (right).

Considering System I, a stiff inclusion with a width $w = l_{1x}/8$ and a height $h = l_{1y}/4$, which is impenetrable for dislocations, is embedded into the aluminum matrix. The results of the distribution of the plastic slip γ regarding different boundary conditions for the numerical system are shown in Figure 5 with respect to the symmetry line at $l_x/2$.

Figure 5 (left) shows the plastic slip incorporating periodic boundary conditions for the mechanical degrees of freedom and for the dislocations. Mimicking grain boundaries, Figure 5 (right) gives the results for mechanically free edges and impenetrable boundaries for the dislocations. This inserts a strong inhomogeneity. Here, we recognize an accumulation of plastic strain above and below the inclusion.

Starting with SSDs only, we observe an increasing amount of geometrically necessary dislocation density. Considering periodic boundary conditions at the left and the right border, the diagrams in Figure 6 depict the evolution in time of ρ_{tot} and ρ_{GND} at a cut through the middle of the system at $l_y/2$, respectively.
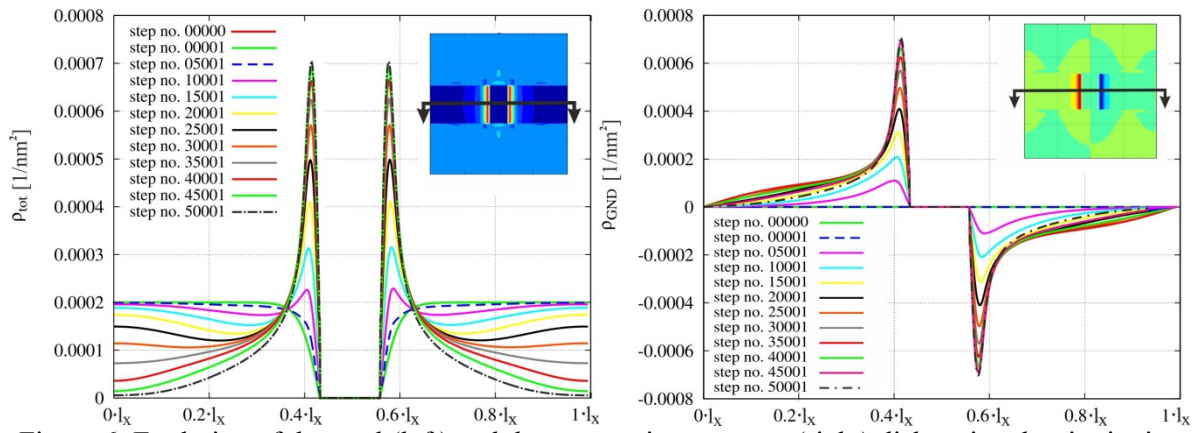

Figure 6: Evolution of the total (left) and the geometric necessary (right) dislocation density in time. Cut through the middle of the system at $l_y/2$.

For the results of the total dislocation density in Figure 6, we recognize a decreasing dislocation density in the field and a pile-up in the vicinity of the inclusion. In Figure 6 (right), the geometrically necessary density start with $\rho_{GND} = 0$ and increases with the evolution. Finally, we observe pile-ups of opposite sign at the left and the right interface to the inclusion.

If we change the shape of the inclusion, keeping a constant volume fraction $(h1 \cdot w1)/(l_{1y} \cdot l_{1x}) = 0.0625$ and vary the dimensions h_1 and w_1 of the inclusion, the system behavior also changes. The diagram in Figure 7 shows the external stress - plastic strain behavior for different inclusion shapes.
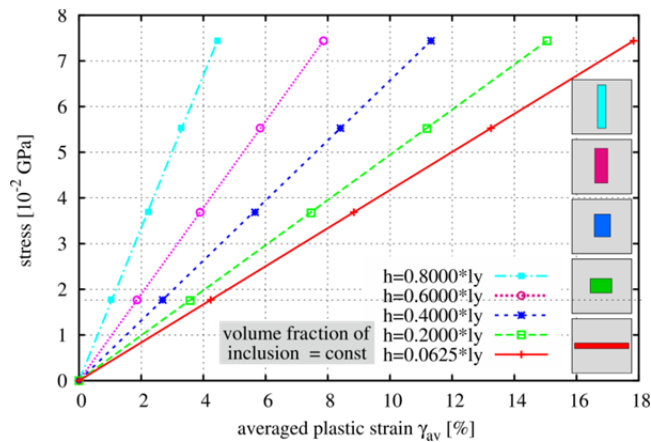

Figure 7: Stress-strain diagram with variation of the inclusion shape at constant volume fraction of the inclusion.

Here, we choose the averaged value of the plastic slip γ_{av} with $\gamma_{av} = \frac{1}{A} \int_A \gamma \, dA$ as representative parameter for the plastic strain. Neglecting the elastic part by $\tau_y = 0$, the results show a linear hardening behavior depending on the inclusion height.

Changing the cutoff of the material and analyzing a system incorporating five inclusions (System II: $w \approx l_{2x}/3$ and $h \approx l_{2y}/3$; System III: $w = l_{2x}/4$ and $h = l_{2y}/2$), the inhomogeneity of the dislocation distribution increases. Figure 8 depicts the results for System II and System III showing the distributions of the geometrically necessary dislocation density and the plastic slip.

Geometrically neccessary dislocation density
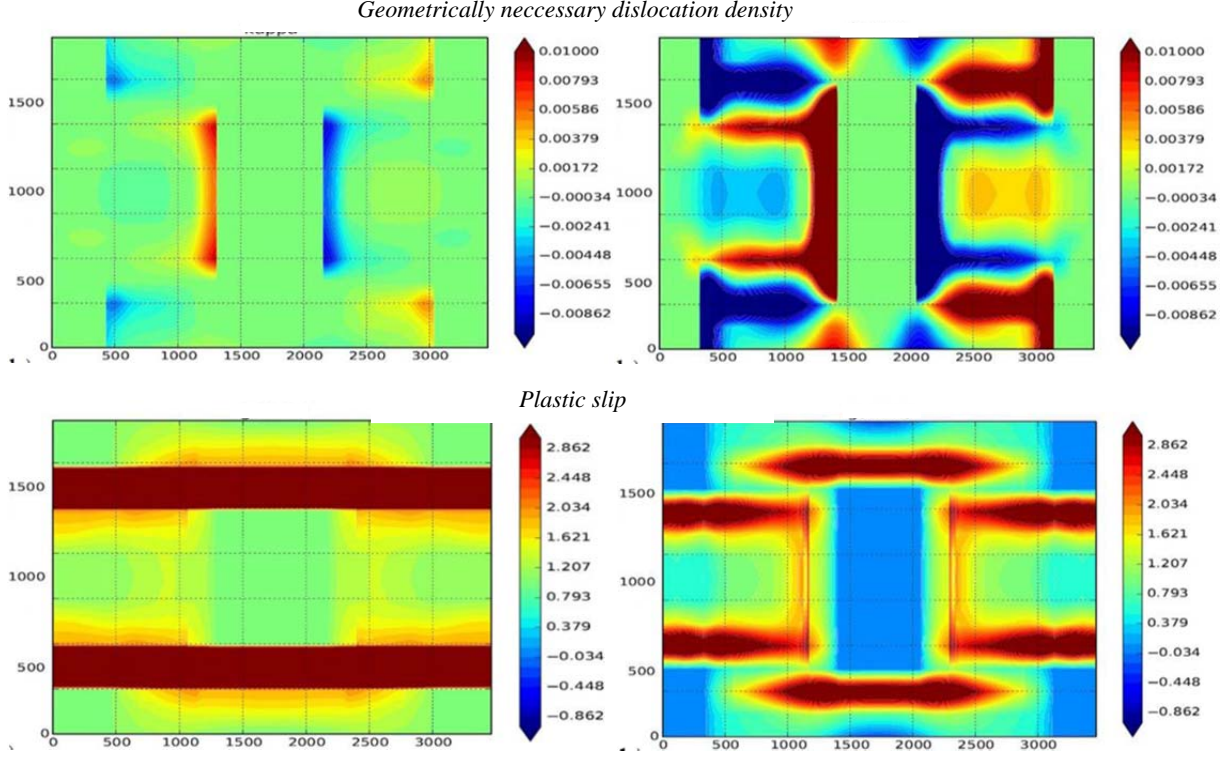

Plastic slip

Figure 8: Distribution of the geometrically necessary dislocations and the plastic slip for System II (left) and System III (right).

It can be seen, that the more the paths of the dislocation motion are hindered, the stronger are the dislocation pile-ups, which causes stress concentrations.

4 DISCUSSION

The present results indicate that damage evolution of metallic glass particle reinforced MMCs presented in this study occurs in several steps and that the inherent damage mechanisms differ. Experimental investigations showed that first cracks form within the matrix material starting at silicon primary crystals. These cracks get larger and wider with higher elongations and partly merge to macroscopic cracks which are mostly orientated along the loading direction. Only few cracks in the metallic glass particles were observed at high elongations. The interface between the metallic glass platelets and the matrix material remained mostly intact which is explained by the good bonding between metallic glass and matrix as shown by Cytron et al. [12] and Lee et al. [9]. These results indicate that plastic deformation mainly takes place within the AlSi12 matrix. A further evidence for this assumption is the formation of matrix extrusions on the edges of metallic glass platelets. The extrusions may be due to dislocation pile-ups leading to stress concentrations and therefore to crack formation around the extrusions as shown in Figure 3 (d).

The microstructural observations during mechanical loading described above are qualitatively in good coincidence with the numerical predictions based on the modelling by a dislocation-based continuum formulation. The numerical analyses predicted a high level of dislocation slip activity, i.e. plas-

tic deformation, close to the edges of the inclusions (cf. Figure 8). In fact, in this region of the metallic platelets extrusions could be observed indicating such dislocation slip activity.

Nevertheless, the model presented deals with rather small inclusions in comparison to the platelets, therefore further investigations should comprise a variation of not only the platelet shape but also the platelet size. On the other hand, a reduction of the platelet size for the experimental investigations may lead to a further increase in reinforcement volume content and hence improve the mechanical properties.

5   CONCLUSIONS

In this contribution, innovative metallic glass particle reinforced MMCs produced by gas pressure infiltration were examined with regard to damage mechanisms and crack evolution. Investigations were performed by in-situ compression tests within a SEM chamber for a detailed investigation of the damage evolution and by numerical modelling.

Experimental results show that first cracks form in the AlSi12 matrix within silicon primary crystals and eutectic silicon lamellae. These cracks get larger with higher elongations and form macroscopic cracks within the matrix material. Plastic deformation was observed to localize in front of metallic glass particles as matrix extrusions. Only few cracks formed in a metallic glass platelet and the bonding in the interface between metallic glass platelet and matrix material remained mostly intact.

A dislocation-based continuum formulation was adapted to the microstructure to investigate the interfacial behavior between the hard amorphous particles and the surrounding aluminum matrix. Looking at different cut-offs of the simplified material, the main deformation mechanisms have been investigated. Considering dislocation pile-ups in the microstructures, the corresponding stress peaks could be identified. The analysis of the distribution of plastic slip over the structure showed the strongly inhomogeneous matrix behaviour during the loading process.

REFERENCES

[1]   M.M. Trexler, N.N. Thadhani, Mechanical properties of bulk metallic glasses, *Progress in Materials Science,* **55**, 2010, pp. 759–839.

[2]   T. Zhang, A. Inoue, New Bulk Glassy Ni-Based Alloys with High Strength of 3000 MPa, *Materials Transactions*, **43**, 2002, pp. 708–711.

[3]   A. Inoue, B.L. Shen, C.T. Chang, Fe- and Co-based bulk glassy alloys with ultrahigh strength of over 4000MPa, *Intermetallics*, **14**, 2006, pp. 936–944.

[4]   A. Inoue, B. Shen, H. Koshiba, H. Kato, A.R. Yavari, Cobalt-based bulk glassy alloy with ultrahigh strength and soft magnetic properties, *Nature materials*, **2**, 2003, pp. 661–663.

[5]   W.L. Johnson, Bulk Glass-Forming Metallic Alloys: Science and Technology, *MRS Bull.*, **24**, 1999, pp. 42–56.

[6]   S. Scudino, K.B. Surreddi, S. Sager, M. Sakaliyska, J.S. Kim, W. Löser, J. Eckert, Production and mechanical properties of metallic glass-reinforced Al-based metal matrix composites, *J Mater Sci*, **43**, 2008, pp. 4518–4526.

[7]   P. Yu, K. Kim, J. Das, F. Baier, W. Xu, J. Eckert, Fabrication and mechanical properties of Ni–Nb metallic glass particle-reinforced Al-based metal matrix composite, *Scripta Materialia*, **54**, 2006, pp. 1445–1450.

[8]   M. Lee, D. Bae, W. Kim, D. Kim, Ni-Based Refractory Bulk Amorphous Alloys with High Thermal Stability, *Materials Transactions*, **44**, 2003, pp. 2084–2087.

[9]   M.H. Lee, J.-H. Kim, J.S. Park, J.C. Kim, W.T. Kim, D.H. Kim, Fabrication Ni-Nb-Ta metallic glass reinforced Al-based alloy matrix composites by infiltration casting process, *Scripta Materialia*, **50**, 2004, pp. 1367-1371.

[10] K. Lichtenberg, K.A. Weidenmann, Innovative aluminum based metallic glass particle reinforced MMCs produced by gas pressure infiltration, *Proceedings of the 20. Symposium Verbundwerkstoffe und Werkstoffverbunde, Vienna, Austria, Juli 3-5, 2015*, accepted.

[11] S. Scudino, K.B. Surredi, S. Sager, M. Sakaliyska, J.S. Kim, W. Löser, J. Eckert, Production and mechanical properties of metallic glass-reinforced Al-based metal matrix composites, *Journal of Material Science*, **43**, 2008, pp. 4518-4526.

[12] S.J. Cytron, a metallic glass-metal matrix composite, *Journal of Materials Science Letters*, **1**, 1982, pp. 211-213.

[13] S. Scudino, G. Liu, K.G. Prashanth, B. Bartusch, K.B. Surreddi, B.S. Murty, J. Eckert, Mechanical properties of Al-based metal matrix composites reinforced with Zr-based glassy particles produced by powder metallurgy, *Acta Materialia*, **57**, 2009, p.2029-2039.

[14] E. Kröner, *Kontinuumstheorie der Versetzungen und Eigenspannungen*, Springer, 1958.

[15] T. Hochrainer, M. Zaiser, P. Gumbsch, A three-dimensional continuum theory of dislocation systems: kinematics and mean-field formulation, *Phil. Mag.* **87**, 2007, pp.1261–1282.

[16] K. Schulz, D. Dickel, S. Schmitt, S. Sandfeld, D. Weygand, P. Gumbsch, Analysis of Dislocation Pile-ups Using a Dislocation-Based Continuum Theory**.** *Modelling Simul. Mater. Sci. Eng.*, **22**, 2014, 025008 (15pp).

[17] E. Van der Giessen, A. Needleman, Discrete dislocation plasticity: a simple planar model, *Modelling Simul. Mater. Sci. Eng.* **3**, 1995, pp.689–735.

[18] H. H. M. Cleveringa, E. VanderGiessen, A. Needleman, Comparison of discrete dislocation and continuum plasticity predictions for a composite material, *Acta Mater.* **45**, 1997, pp.3163 – 3179.

[19] H. H. M. Cleveringa, E. VanderGiessen, A. Needleman, A discrete dislocation analysis of residual stresses in a composite material, *Phil. Mag.* **79**, 1999, pp.893–920.

[20] C. Schwarz, R. Sedlácek, E. Werner, Plastic deformation of a composite and the source-shortening e_ect simulated by the continuum dislocation based model., *Modelling Simul. Mater. Sci. Eng.* **15**, 2007, pp.37 – 49.

[21] S. Yefimov, I. Groma, E. VanderGiessen, A comparison of a statistical mechanics based plasticity model with discrete dislocation plasticity calculations, *J. Mech. Phys. Solids* **52**, 2004, pp.279–300.

[22] T. Hochrainer, S. Sandfeld, M. Zaiser, P. Gumbsch, Continuum dislocation dynamics: towards a physical theory of crystal plasticity. *J. Mech. Phys. Solids*, **63**, 2014, pp.167-178.

[23] M. Merzkirch, C. Blümel, R. Rössler, K.G. Schell, E.C. Bucharsky, K.A. Weidenmann, Manufacturing and Characterization of Interpenetrating SiC Lightweight Composites, *Procedia CIRP*, **18**, 2014, pp. 102–107.

[24] I. Groma, F. Csikor, M. Zaiser, Spatial correlations and higher-order gradient terms in a continuum description of dislocation dynamics, *Acta Mater.* **51**, 2003, pp.1271–1281.

[25] M. Zaiser, N. Nikitas, T. Hochrainer, E. Aifantis, Modelling size effects using 3D density-based dislocation dynamics, *Phil. Mag.* **87**, 2007, pp.1283–1306.